Computers and Mathematics with Applications 61 (2011) 1739–1753

Contents lists available at ScienceDirect

Computers and Mathematics with Applications

journal homepage: www.elsevier.com/locate/camwa

Enhanced natural convection in an isosceles triangular enclosure filled with a nanofluid

S.M. Aminossadati [a,*], B. Ghasemi [b]

[a] The University of Queensland, School of Mechanical and Mining Engineering, QLD 4072, Australia

[b] Shahrekord University, Faculty of Engineering, P.O. Box 115, Shahrekord, Iran

ARTICLE INFO

Article history:
Received 9 October 2009
Received in revised form 21 January 2011
Accepted 2 February 2011

Keywords:
Isosceles triangular enclosure
Natural convection
Nanofluid
Heat source

ABSTRACT

Natural convection is studied in an isosceles triangular enclosure with a heat source located at its bottom wall and filled with an Ethylene Glycol–Copper nanofluid. This paper examines the effects of pertinent parameters such as the Rayleigh number, the solid volume fraction, the heat source location, and the enclosure apex angle on the thermal performance of the enclosure. The thermal performance of the enclosure is improved with an increase in the Rayleigh number and solid volume fraction. The results also show that the variation of heat transfer rate with respect to the enclosure apex angle and heat source position and dimensions is different at low and high Rayleigh numbers. A comparison is also presented between the results obtained from the modified and original Maxwell models. The results show that the heat transfer is generally higher based on the modified Maxwell model.

1. Introduction

In recent years, the number of studies conducted on natural convection in triangular enclosures has increased, as evidenced by the research articles cited in [1–3]. The increased interest in natural convection is due to its application in various environmental, geophysical and engineering problems. In particular, natural convection has been considered an effective and economical cooling strategy for electronic devices [4,5]. However, miniaturisation of components in modern electronic devices is subject to strict space and weight constraints, which in turn results in increased heat dissipation per unit area [6,7]. Therefore, an enhanced cooling strategy is needed to avoid premature failure of miniaturised electronic components and to ensure their reliability and life expectancy.

If the cooling strategy utilises a coolant fluid with a low thermal conductivity, the natural convection flow field only acquires a limited strength. It is, therefore, of fundamental interest to explore innovative and practical strategies that strengthen the natural convection flow for various geometries of electronic components. Bergles [8] described nine techniques for heat transfer enhancement, among which the addition of liquid droplets or solid particles in the base convective fluid was a promising technique for natural convection enhancement. Ridouane and Campo [9] analysed the natural convection in an isosceles triangular enclosure and showed that if it was filled with a mixture of different gases, it had a higher cooling performance than if filled with air.

For the first time, Choi [10] suggested that the addition of nanoparticles into the base convective fluid increases its thermal conductivity and therefore substantially enhances its heat transfer characteristics. The resulting mixture of nanoparticles and the base convective fluid is referred to as a nanofluid. Some researchers have shown that the use of water-based nanofluids enhances the natural convection in inclined enclosures [11–14]. The influence of nanofluids on

* Corresponding author. Tel.: +61 7 33653676; fax: +61 7 33653888.
E-mail address: uqsamino@uq.edu.au (S.M. Aminossadati).

0898-1221/$ – see front matter © 2011 Elsevier Ltd. All rights reserved.
doi:10.1016/j.camwa.2011.02.001

Nomenclature

C_p	Specific heat, J kg^{-1} K^{-1}
d	Heat source distance from the left vertex, m
D	Dimensionless heat source distance from the left vertex (d/L)
g	Gravitational acceleration, m s^{-2}
h	Heat source height, m
H	Dimensionless heat source height (h/L)
h_{nl}	Thickness of nano-layer, nm
k	Thermal conductivity, W m^{-1} K^{-1}
L	Length of enclosure bottom wall, m
Nu	Local Nusselt number on the heat source
Nu$_m$	Average Nusselt number
p	Fluid pressure, Pa
$\overline{p}$	Modified pressure ($p + \rho_c g y$)
P	Dimensionless pressure ($\overline{p}L^2/\rho_{nf}\alpha_f^2$)
Pr	Prandtl number (ν_f/α_f)
r_{np}	Radius of nanoparticles, nm
Ra	Rayleigh number ($g\beta_f L^3(T_h - T_c)/\nu_f\alpha_f$)
T	Temperature, K
u, v	Velocity components in x, y directions, m s^{-1}
U, V	Dimensionless velocity components (uL/α_f, vL/α_f)
$\vec{V}$	Dimensionless velocity vector
w	Heat source length, m
W	Dimensionless heat source length (w/L)
x, y	Cartesian coordinates, m
X, Y	Dimensionless coordinates (x/L, y/L)

Greek symbols

α	Thermal diffusivity, m^2 s^{-1}
β	Thermal expansion coefficient, K^{-1}
δ	Apex angle of the triangular enclosure (°)
ϕ	Solid volume fraction
μ	Dynamic viscosity, N s m^{-2}
ν	Kinematic viscosity, m^2 s^{-1}
θ	Dimensionless temperature $(T - T_c)/(T_h - T_c)$
ρ	Density, kg m^{-3}
ψ	Stream function

Subscripts

c	Cold wall
eff	Effective
eq	Equivalent
f	Fluid (pure)
h	Heat source
L	Left side
nf	Nanofluid
nl	Nano-layer
np	Nanoparticle
R	Right side
T	Top side.

heat transfer performance is still a controversial issue. It has been demonstrated that the augmentation or mitigation of heat transfer depends upon the theoretical models used to determine the nanofluid properties such as dynamic viscosity and thermal conductivity [15,16]. Some of the models include the contribution of Brownian motion of the nanoparticles to determine the nanofluid properties [17–19]. However, there are still a number of studies which rely on either original Maxwell model [20] or modified Maxwell model [21].

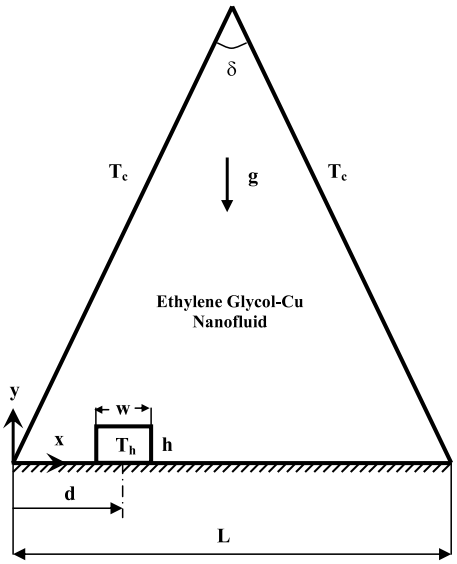

Fig. 1. A schematic diagram of the physical model.

Table 1
Physical properties of Cu and Ethylene Glycol [31,32].

	ρ(kg m^{-3})	C_P (J kg^{-1} K^{-1})	k (W m^{-1} K^{-1})	β (K^{-1})
Copper (Cu)	8933	385	401	1.67×10^{-5}
Ethylene Glycol ($C_2H_6O_2$)	1109	2400	0.26	6.5×10^{-4}

The conductors in the electrical engineering industry often have the form of a prism of triangular cross-section. Triangular-shaped enclosures can also be found in the electronic equipment such as the power transistors, the printed wiring boards and the chip packages mounted on computer motherboards. In particular, a triangular-shaped chip package mounted on a motherboard is used to dissipate heat from the motherboard. This can be modelled by considering a triangular enclosure with a heat source located at the bottom wall. Recently, many researchers have studied natural convection in isosceles triangular enclosures filled with a fluid having a low thermal conductivity [22–30]. The heat transfer of the triangular enclosures can be enhanced by improving the thermal properties of the working fluid. To the best knowledge of the authors, the literature is scarce in the field of heat transfer enhancement as a result of using nanofluids in isosceles triangular enclosures. As such, the purpose of this paper is to provide steady-state numerical results for natural convection in an isosceles triangular enclosure filled with an Ethylene Glycol–Copper (EG–Cu) nanofluid. The results of the simulation are presented in terms of pertinent parameters such as the Rayleigh number, solid volume fraction, position and dimensions of the heat source and the apex angle of the triangular enclosure.

2. Problem description

The present model consists of an isosceles triangular enclosure filled with an EG–Cu nanofluid (Fig. 1). A heat source with a length of w and a height of h and with a relatively high temperature (T_h) is located at the thermally insulated bottom wall, while the inclined walls of the enclosure are maintained at a relatively lower temperature (T_c). It is assumed that EG and Cu nanoparticles are in thermal equilibrium, the nanofluid is Newtonian and incompressible, the flow is laminar and radiation effects are negligible. Constant thermophysical properties are considered for the nanofluid except for the density variation in the buoyancy forces determined by using the Boussinesq approximation. The thermophysical properties of EG and Cu are given in Table 1.

3. Governing equations

The governing equations of continuity, momentum and energy can be written in non-dimensional forms as shown in Eqs. (1)–(4)

$$\vec{\nabla}.\vec{V} = 0 \tag{1}$$

$$\vec{V}.\vec{\nabla}U = -\frac{\partial P}{\partial X} + \frac{\mu_{nf}}{\rho_{nf}\alpha_f}(\nabla^2 U) \tag{2}$$

Table 2
Applied formulae for the nanofluid properties.

Nanofluid properties	Applied model
Density	$\rho_{nf} = (1-\phi)\rho_f + \phi\rho_{np}$
Thermal diffusivity	$\alpha_{nf} = k_{\text{eff}}/(\rho C_p)_{nf}$
Heat capacitance	$(\rho C_p)_{nf} = (1-\phi)(\rho C_p)_f + \phi(\rho C_p)_{np}$
Thermal expansion coefficient	$(\rho\beta)_{nf} = (1-\phi)(\rho\beta)_f + \phi(\rho\beta)_{np}$
Dynamic viscosity [33]	$\mu_{nf} = \frac{\mu_f}{(1-\phi)^{2.5}}$

$$\vec{V}.\vec{\nabla}V = -\frac{\partial P}{\partial Y} + \frac{\mu_{nf}}{\rho_{nf}\alpha_f}(\nabla^2 V) + \frac{(\rho\beta)_{nf}}{\rho_{nf}\beta_f}\text{Ra}\,\text{Pr}\,\theta \tag{3}$$

$$\vec{V}.\vec{\nabla}\theta = \frac{\alpha_{nf}}{\alpha_f}\nabla^2\theta \tag{4}$$

where, the following non-dimensional groups are used in the analysis:

$$X = \frac{x}{L}, \quad Y = \frac{y}{L}, \quad U = \frac{uL}{\alpha_f}, \quad V = \frac{vL}{\alpha_f}, \quad P = \frac{\bar{p}L^2}{\rho_{nf}\alpha_f^2}$$
$$\theta = \frac{T-T_c}{T_h-T_c}, \quad \text{Ra} = \frac{g\beta_f L^3(T_h-T_c)}{\nu_f\alpha_f}, \quad \text{Pr} = \frac{\nu_f}{\alpha_f}. \tag{5}$$

The non-dimensional boundary conditions are as follows:

- Along all the walls of the enclosure $U = V = 0$
- Along the horizontal side of the enclosure $\partial\theta/\partial Y = 0$ (6)
- Along the inclined sides of the enclosure $\theta = 0$.

4. Nanofluid properties

The thermophysical properties of the EG–Cu nanofluid are determined using the formulae presented in Table 2. The effective thermal conductivity of the nanofluid is also determined based on the modified Maxwell model applied by Yu and Choi [21]. In addition, a comparison study is presented between the results obtained from the modified and the original Maxwell models.

4.1. Original Maxwell model

According to the original Maxwell model [20], the thermal conductivity of EG–Cu nanofluid (k_{eff}) for spherical Cu nanoparticles is

$$k_{\text{eff}} = k_f\left[\frac{(k_{np}+2k_f) - 2\phi(k_f - k_{np})}{(k_{np}+2k_f) + \phi(k_f - k_{np})}\right] \tag{7}$$

where, k_{np} is the thermal conductivity of dispersed Cu nanoparticles and k_f is the thermal conductivity of pure EG. This classical model has been cited by many researchers [34–36]. However, it does not take into account the Brownian motion of nanoparticles and the effect of solid-like nano-layers formed around nanoparticles.

4.2. Modified Maxwell model

The modified Maxwell model takes into account a nano-layer with a solid-like structure formed by the liquid molecules close to a solid surface. According to this model, the thermal conductivity of the EG–Cu nanofluid (k_{eff}) having spherical Cu nanoparticles is

$$k_{\text{eff}} = k_f\left[\frac{(k_{eq}+2k_f) + 2(k_{eq}-k_f)(1+\sigma)^3\phi}{(k_{eq}+2k_f) - (k_{eq}-k_f)(1+\sigma)^3\phi}\right]. \tag{8}$$

In this equation, σ is the ratio of the thickness of nano-layer to the original radius of nanoparticles (h_{nl}/r_{np}), k_f is the thermal conductivity of pure fluid, ϕ is the solid volume fraction of the nanofluid and k_{eq} is the equivalent thermal conductivity of nanoparticles and their layers:

$$k_{eq} = k_{np}\left[\gamma\frac{2(1-\gamma) + (1+\sigma)^3(1+2\gamma)}{-(1-\gamma) + (1+\sigma)^3(1+2\gamma)}\right]. \tag{9}$$

In this equation, γ is the ratio of thermal conductivity of nano-layers upon the thermal conductivity of the nanoparticles ($\gamma = k_{nl}/k_{np}$). In this study, it is assumed that $h_{nl} = 2$ nm, $r_{np} = 3$ nm and $k_{nl} = 100k_f$. Yu and Choi [21] argued that for these conditions, the results of the modified Maxwell model are in good agreement with the experimental results.

5. Numerical approach

The governing equations (1)–(4) with the corresponding boundary conditions given in Eq. (6) are solved based on the control volume formulation and the SIMPLE algorithm [37]. The power-law scheme is used to discretise the convection–diffusion terms. The resulting algebraic equations are numerically solved in FORTRAN. A regular rectangular domain with uniform grid is first generated. Then, the triangular model is developed by approximating the inclined walls of the triangular enclosure with staircase-like zigzag lines [1,26] and inactivating the grid cells outside of the triangular domain.

Other useful quantities such as Nusselt number for each side of the heat source can be determined after solving the governing equations for U, V and θ. The local Nusselt numbers for the left, right and top sides of the heat source are defined as

$$\mathrm{Nu}_L = +\frac{k_{\mathrm{eff}}}{k_f}\frac{\partial\theta}{\partial X}\bigg|_{\text{Left side}} \tag{10}$$

$$\mathrm{Nu}_R = -\frac{k_{\mathrm{eff}}}{k_f}\frac{\partial\theta}{\partial X}\bigg|_{\text{Right side}} \tag{11}$$

$$\mathrm{Nu}_T = -\frac{k_{\mathrm{eff}}}{k_f}\frac{\partial\theta}{\partial Y}\bigg|_{\text{Top side}}. \tag{12}$$

Thus, the average Nusselt number for each side of the heat source is determined by integrating the local Nusselt number along the surface of each side of the heat source

$$\mathrm{Nu}_{m,L} = \frac{1}{H}\int_0^H \mathrm{Nu}_L.\mathrm{d}Y \tag{13}$$

$$\mathrm{Nu}_{m,R} = \frac{1}{H}\int_0^H \mathrm{Nu}_R.\mathrm{d}Y \tag{14}$$

$$\mathrm{Nu}_{m,T} = \frac{1}{W}\int_{D-\frac{W}{2}}^{D+\frac{W}{2}} \mathrm{Nu}_T.\mathrm{d}X. \tag{15}$$

The total average Nusselt number (Nu_m) for the heat source can be obtained by integrating the local Nusselt numbers along the left, right and top sides of the heat source.

$$\mathrm{Nu}_m = \frac{1}{2H+W}\left[\int_0^H \mathrm{Nu}_L.\mathrm{d}Y + \int_{D-\frac{W}{2}}^{D+\frac{W}{2}} \mathrm{Nu}_T.\mathrm{d}X + \int_0^H \mathrm{Nu}_R.\mathrm{d}Y\right]. \tag{16}$$

The variation of average Nusselt number (Nu_m) for seven different grid sizes is examined to study the independence of the solution to the grid size. Three different apex angles of 60°, 90° and 120° are considered and the results for $\mathrm{Ra} = 10^5$, $D = 0.5$, $W = H = 0.1$, and $\phi = 0.05$ are presented in Fig. 2. A grid size of 100×100 is found to meet the requirements of both the grid independence study and the computational time limits. The convergence criterion is to reduce the maximum mass residual of the grid control volume below 10^{-8}.

The present numerical approach is validated against the study developed by Varol et al. [38]. The results of this validation for a right triangular enclosure with a heat source (T_h) located in the middle of its vertical wall are presented in Fig. 3. The present numerical code has also been validated for enclosures filled with nanofluids and the results have been reported in the literature [39–41].

6. Results

In the present analysis, the Prandtl number is assumed to be $\mathrm{Pr} = 151$, and the Rayleigh number (Ra), the solid volume fraction (ϕ), the enclosure apex angle (δ), the heat source position (D), the heat source length (W), and the heat source height (H) are assumed to be in the following ranges: $10^3 \le \mathrm{Ra} \le 10^6$, $0 \le \phi \le 0.05$, $60^\circ \le \delta \le 140^\circ$, $0.2 \le D \le 0.5$, $0.05 \le W \le 0.7$, and $0.02 \le H \le 0.2$.

6.1. Rayleigh number and solid volume fraction

In this section, the effects of Rayleigh number (Ra) and solid volume fraction (ϕ) on the heat transfer performance of the enclosure are studied. It is assumed that $D = 0.5$, $\delta = 90^\circ$, and $H = W = 0.1$. Fig. 4 presents the streamlines (left) and isotherms (right) for both the EG–Cu nanofluid with $\phi = 0.05$ (—) and the pure EG (— — —) at three different Rayleigh numbers ($\mathrm{Ra} = 10^4$, 10^5 and 10^6). Symmetrical flow and temperature fields with respect to the vertical median of the

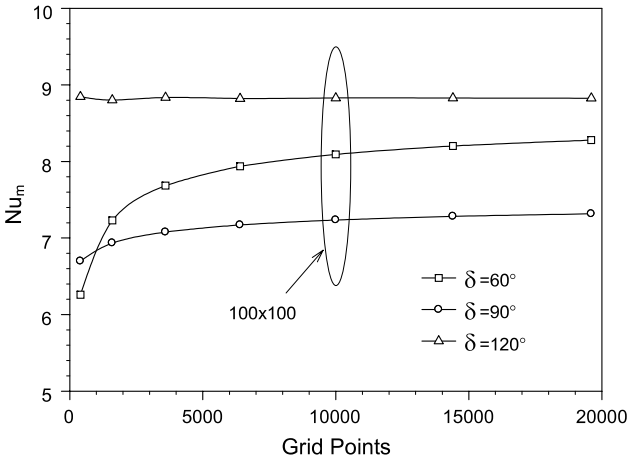

Fig. 2. Grid independence study (Ra $= 10^5$, $\phi = 0.05$, $D = 0.5$, $W = H = 0.1$).

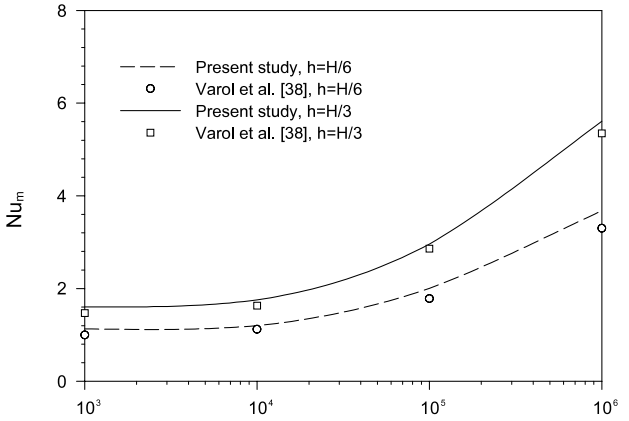

Fig. 3. Code validation: a comparison of the present study against Varol et al. [38].

enclosure can be observed for all values of Ra. The symmetry in the flow and temperature fields is related to the heat source being located at the centreline of the bottom wall. The streamlines indicate two counter-rotating circulating cells, rotating clockwise in the right section and counter-clockwise in the left section of the enclosure. The flow rises along the mid-plane of the enclosure, on which the heat source is located, and descends along the inclined walls, which have a relatively lower temperature. As Ra increases, the buoyant forces become stronger and therefore the absolute value of the stream function for both the EG–Cu nanofluid and the pure EG increases. A comparison study between the EG–Cu nanofluid and the pure EG indicates that at high Ra, circulating cells for EG–Cu nanofluid are stronger than those for pure EG, whereas at low Ra, the pure EG has stronger circulating cells. At low Ra, the isotherms are uniformly distributed in the enclosure, showing that conduction dominates the heat transfer. However, as Ra increases, an irregularity is observed within the temperature field, and the intensity of the isotherms increases near the heat source. This is an indication of strengthening of the buoyant forces and convection heat transfer in the enclosure.

The variations in the vertical component of velocity (V) and the dimensionless temperature (θ) of the flow, along a horizontal axis extending over the top side of the heat source ($Y = 0.1$), are plotted in Figs. 5a and 5b, respectively. These graphs provide a better understanding of the flow behaviour within the enclosure for both the EG–Cu nanofluid and the pure EG at different Ra. An examination of the magnitude of V and θ at different Ra confirms the results previously obtained from analysing the streamlines and isotherms. The V profiles verify the existence of clockwise and anti-clockwise circulating cells within the enclosure. The increase of the magnitude of V with the increase of Ra is an indication of stronger buoyant flows within the enclosure at high Ra. The heat transfer mechanism is, therefore, expected to be due to convection at high Ra, while conduction is responsible for the heat transfer at low Ra. The θ profiles show that the fluid temperature along the $Y = 0.1$ axis increases from the left wall towards the heat source. At any point along this axis, the temperature decreases as Ra increases. The results also show that for Ra $= 10^6$ and away from the heat source, the EG–Cu nanofluid is associated with a higher absolute magnitude of velocity and a lower temperature compared to the pure EG due to stronger buoyant flows at high Rayleigh numbers.

The heat transfer rate is studied in terms of the average Nusselt number (Nu_m) calculated along the sides of the heat source. Fig. 6 presents the variation of Nu_m with respect to the solid volume fraction of nanofluid (ϕ) at various Ra. For

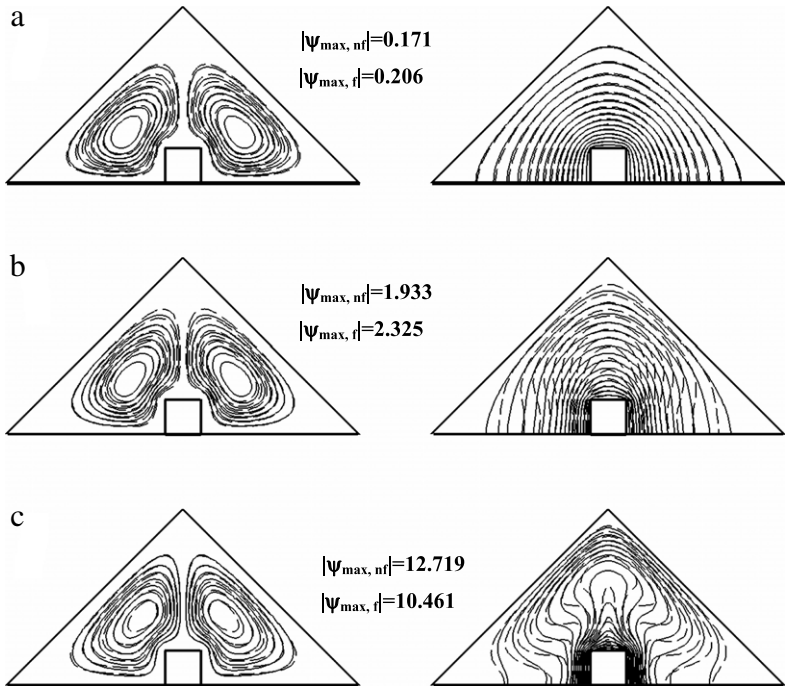

Fig. 4. Streamlines (left) and isotherms (right) for $\delta = 90^\circ$, $D = 0.5$, $W = H = 0.1$, EG–Cu nanofluid with $\phi = 0.05$ (____) and pure EG (− − −), (a) Ra $= 10^4$, (b) Ra $= 10^5$, (c) Ra $= 10^6$.

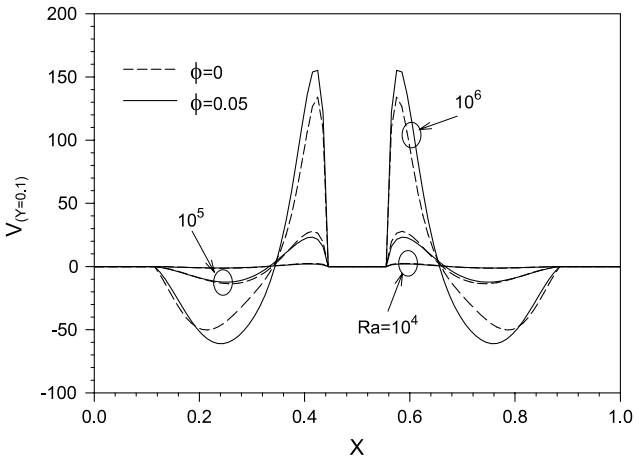

Fig. 5a. Vertical velocity profile at $Y = 0.1$ for both EG–Cu nanofluid and pure EG ($\delta = 90^\circ$, $D = 0.5$, $W = H = 0.1$).

all values of Ra, the average heat transfer rate from the heat source increases as the solid volume fraction increases. This increase is due to the enhancement of the nanofluid effective thermal conductivity as the volume of nanoparticles increases.

6.2. Enclosure apex angle

In this section, the effect of apex angle of the triangular enclosure (δ) on the heat transfer performance of the enclosure is studied. It is assumed that $D = 0.5$, $\phi = 0.05$ and $H = W = 0.1$. Fig. 7 shows the streamlines (left) and the isotherms (right) for Ra $= 10^5$ and three different apex angles ($\delta = 60^\circ$, 90° and 120°). The results show that for all apex angles, two counter-rotating circulating cells are observed within the enclosure. As discussed earlier, at $\delta = 90^\circ$, the circulating cells are symmetrical; however, at $\delta = 60^\circ$ and 120°, that is not the case. The minimum and maximum values of the stream function show that the right circulating cell is stronger than the left circulating cell. This asymmetrical behaviour of the flow field in the isosceles triangular enclosure has also been reported in the literature [25,26]. The asymmetrical results are observed as the flow undergoes a supercritical pitchfork bifurcation when Rayleigh numbers increases above a critical value.

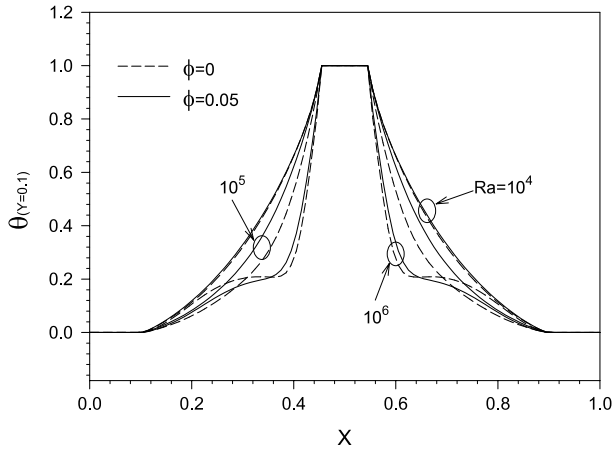

Fig. 5b. Temperature profile at $Y = 0.1$ for both EG–Cu nanofluid and pure EG ($\delta = 90^\circ$, $D = 0.5$, $W = H = 0.1$).

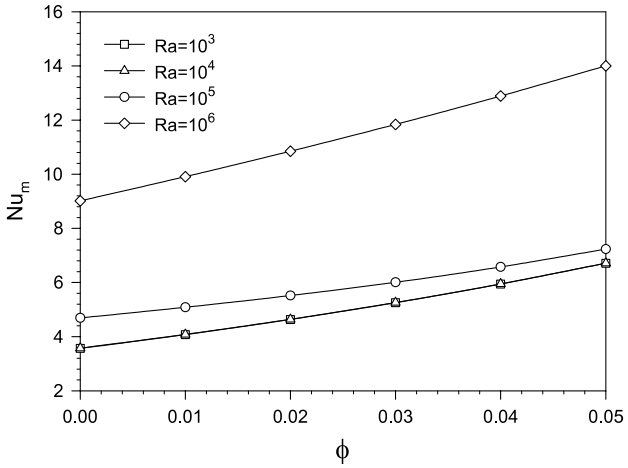

Fig. 6. Variation of Nu_m with ϕ at different Ra ($\delta = 90^\circ$, $D = 0.5$, $W = H = 0.1$).

The asymmetrical flow behaviour, which is observed at apex angles of $\delta = 60^\circ$ and $\delta = 120^\circ$ but not at $\delta = 90^\circ$, can be attributed to the fact that the critical Rayleigh number is a function of the enclosure apex angle [25].

It is also noteworthy that since the length of the bottom wall of the enclosure is kept constant, as the apex angle increases, the enclosure becomes smaller and the circulating cells become more limited. Thus, an increase in the apex angle results in a decrease in the strength of the circulating cells. However, this does not mean that the heat transfer rate will be lower for higher apex angles. It is worth noting that as the apex angle increases, the heat source becomes closer to the cold inclined walls and the conduction heat transfer rate is expected to increase.

Fig. 8 depicts the variation of the average Nusselt number (Nu_m) with the apex angle (δ) for different Ra. At low values of δ, a considerable distance exists between the heat source and the cold inclined walls. Therefore, as Ra increases, the buoyant forces and the convection flow field become stronger and Nu_m increases. However, at higher values of δ, this distance becomes smaller, limiting the strength of the convective flow field. The influence of Rayleigh number on the heat transfer rate proves to be insignificant for $\delta > 120^\circ$. This is due to the limited convective flow circulations within the enclosure at high apex angles.

6.3. Heat source position

In this section, the effect of the heat source position on the heat transfer performance of the enclosure is studied. It is assumed that $\delta = 90^\circ$, $\phi = 0.05$ and $W = H = 0.1$. Fig. 9 depicts the streamlines (left) and the isotherms (right) for $\mathrm{Ra} = 10^5$ and three values of D ($D = 0.2$, 0.3 and 0.4). For $D = 0.2$, a strong circulating cell is observed in the right side of the enclosure and the isotherms are intensified near the left inclined wall. As the heat source moves towards the centre of the bottom wall, another circulating cell starts to develop in the left side of the enclosure and the isotherms spread throughout the enclosure. It is also found that when the heat source is positioned at $D = 0.3$, the maximum absolute value of the stream function for the right circulating cell is obtained.

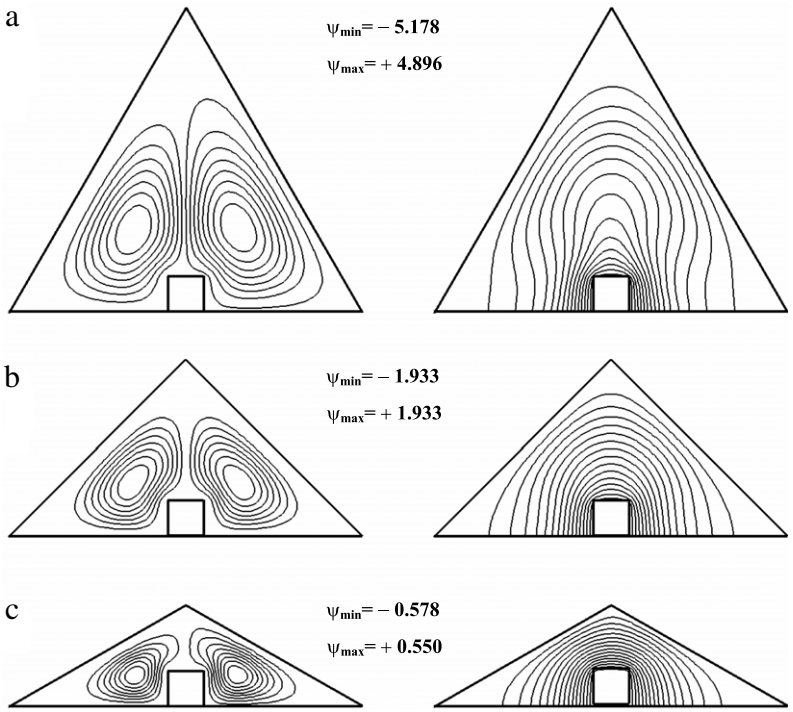

Fig. 7. Streamline (left) and isotherms (right) for Ra $= 10^5$, $\phi = 0.05$, $D = 0.5$, $W = H = 0.1$, (a) $\delta = 60°$, (b) $\delta = 90°$, (c) $\delta = 120°$.

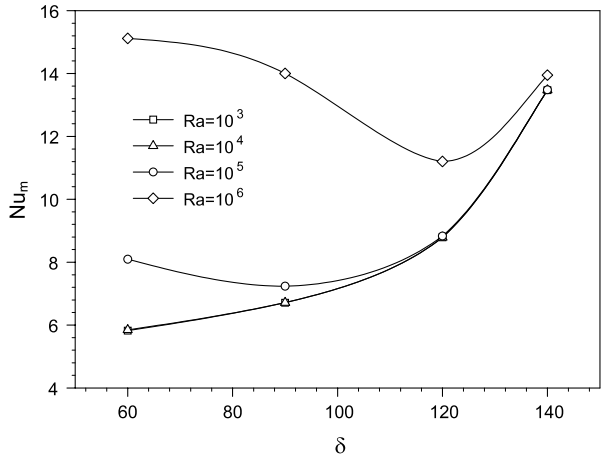

Fig. 8. Variation of Nu_m with δ at different Ra ($\phi = 0.05$, $D = 0.5$, $W = H = 0.1$).

Figs. 10a and 10b present the horizontal component of velocity (U) and the dimensionless temperature (θ), respectively, along the vertical median of the enclosure for Ra $= 10^5$, $\delta = 90°$, $\phi = 0.05$, $W = H = 0$ and for various positions of the heat source. Fig. 10a shows a symmetrical flow about the mid-plane of the enclosure. The velocity of the flow along the mid-plane is zero when the heat source is located at $D = 0.5$. The circulating cell in the left side of the enclosure becomes limited as the heat source moves towards the left side of the bottom wall. As a result, the right circulating cell grows and moves towards the centre of the enclosure. This central circulating cell continues to grow till $D = 0.3$, where it is being affected by the left wall. Thus, the maximum growth of the central circulating cell and the maximum horizontal velocity occur at $D = 0.3$. This is in line with the results obtained for the maximum absolute value of the stream function. For all positions of the heat source, Fig. 10b shows the same temperature for the fluid and the cold inclined walls at $Y = 0.5$. However, the fluid temperature increases as it approaches the heat source located at the bottom wall. At any point on the vertical mid-plane axis, the fluid temperature increases as the heat source approaches the centre of the bottom wall. It is also apparent that the fluid temperature reaches the heat source temperature at $Y = 0.1$ when the heat source is in the centre of the bottom wall.

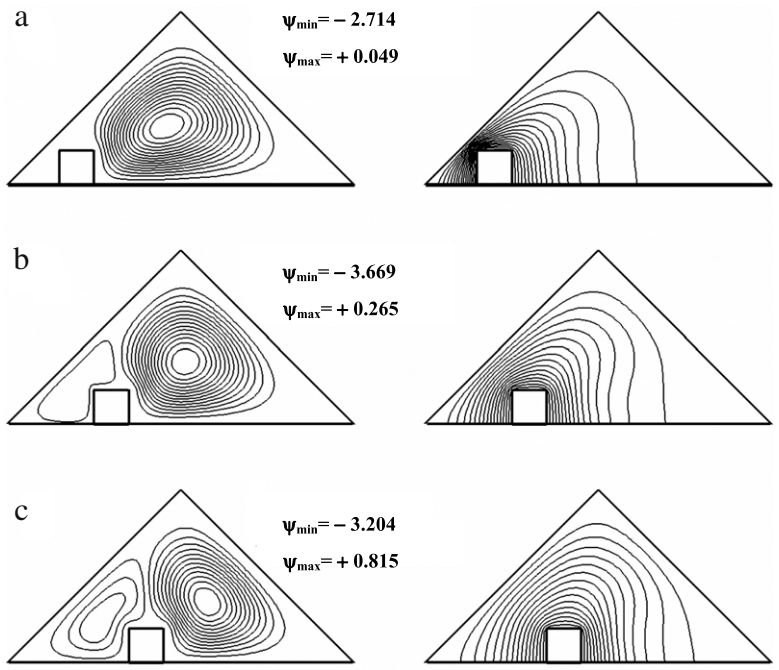

Fig. 9. Streamline (left) and isotherms (right) for Ra $= 10^5$, $\phi = 0.05$, $\delta = 90^\circ$, $W = H = 0.1$, (a) $D = 0.2$, (b) $D = 0.3$, (c) $D = 0.4$.

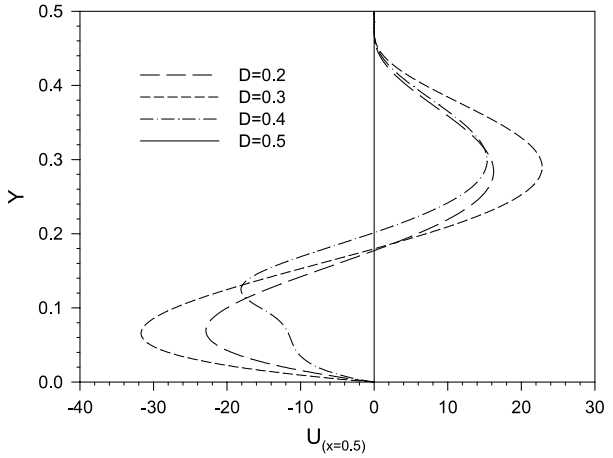

Fig. 10a. Horizontal velocity profile at $X = 0.5$ for different values of D (Ra $= 10^5$, $\delta = 90^\circ$, $\phi = 0.05$, $W = H = 0.1$).

Fig. 11 clearly shows the individual contribution of the left, right and top surfaces of the heat source in the heat transfer process. Fig. 11a shows that for all values of Ra except for Ra $= 10^6$, the Nusselt number calculated on the left side of the heat source ($Nu_{m,L}$) decreases as the heat source moves away from the cold wall. This is because of the reduction in the conduction heat transfer. At Ra $= 10^6$, as D increases, $Nu_{m,L}$ first decreases and then increases due to the strengthening of the buoyant flows. Fig. 11b shows that the Nusselt number calculated on the right side of the heat source ($Nu_{m,R}$) does not significantly change with the variation in D. However, the highest values for $Nu_{m,R}$ are found at Ra $= 10^6$, where a stronger buoyant flow field appears in the enclosure. Fig. 11c shows that the trends for the Nusselt number calculated on the top side of the heat source ($Nu_{m,T}$) are very similar to those for $Nu_{m,L}$. The only interesting point is that $Nu_{m,T}$ has the lowest value for Ra $= 10^5$. This is because of the low strength of the convection flow field on the top side of the heat source, which also prevents the conduction heat transfer for being properly achieved. Finally, Fig. 11d shows the variation in the total average Nusselt number (Nu_m) with respect to D. Nu_m is the average of the Nusselt numbers on the left, right and top sides of the heat source. Therefore, since $Nu_{m,R}$ does not significantly vary with D, Nu_m follows the variation of $Nu_{m,L}$ and $Nu_{m,T}$. This means that as D increases, for Ra $= 10^3$, 10^4, and 10^5, Nu_m continuously decreases, while for Ra $= 10^6$, it reaches its minimum at $D = 0.3$.

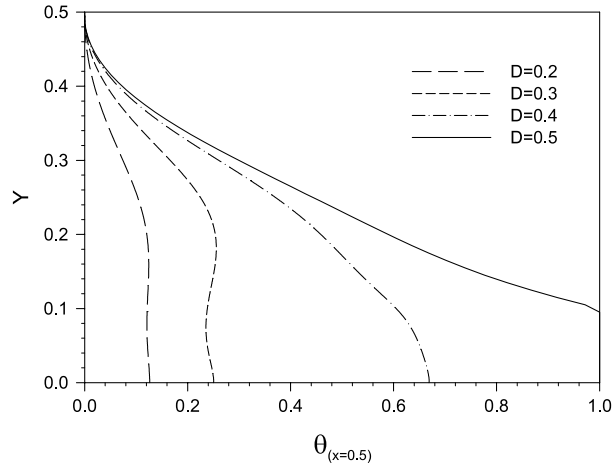

Fig. 10b. Temperature profile at $X = 0.5$ for different values of D ($\mathrm{Ra} = 10^5$, $\delta = 90°$, $\phi = 0.05$, $W = H = 0.1$).

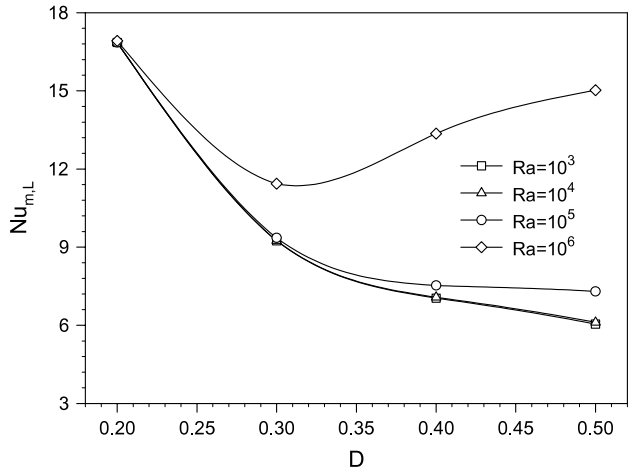

Fig. 11a. Variation of $\mathrm{Nu}_{m,L}$ with D at different Ra ($\delta = 90°$, $\phi = 0.05$, $W = H = 0.1$).

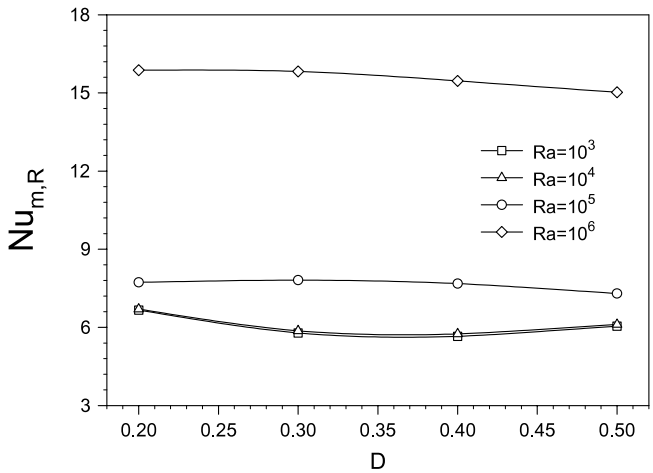

Fig. 11b. Variation of $\mathrm{Nu}_{m,R}$ with D at different Ra ($\delta = 90°$, $\phi = 0.05$, $W = H = 0.1$).

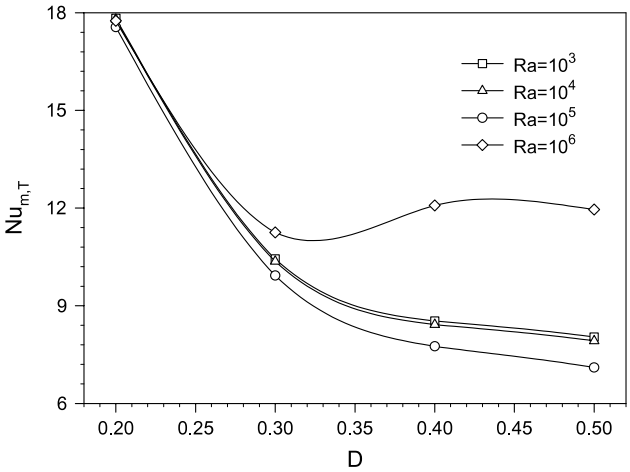

Fig. 11c. Variation of $Nu_{m,T}$ with D at different Ra ($\delta = 90^\circ$, $\phi = 0.05$, $W = H = 0.1$).

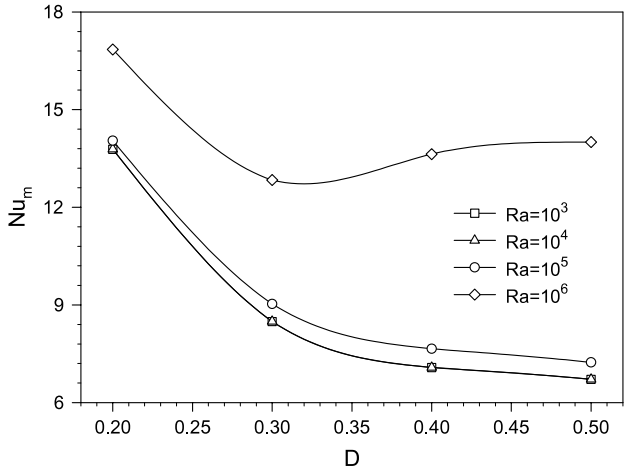

Fig. 11d. Variation of Nu_m with D at different Ra ($\delta = 90^\circ$, $\phi = 0.05$, $W = H = 0.1$).

6.4. Heat source dimensions

In this section, the effect of heat source dimensions on the heat transfer performance of the enclosure is studied. It is assumed that $Ra = 10^5$, $D = 0.5$, $\phi = 0.05$, and $\delta = 90^\circ$. Fig. 12 shows the streamlines (left) and the isotherms (right) for the heat source with $H = 0.1$ and three values of W ($W = 0.05$, 0.3 and 0.7). Even though the apex angle is 90° and the heat source is positioned in the middle of the bottom wall, an asymmetry in the flow patterns is observed for $W = 0.05$. This is in line with the results of Holtzman et al. [25] who studied natural convection within an isosceles triangular enclosure heated from below and symmetrically cooled from above. They showed that for a particular triangular geometry and above the critical Grashof number, the geometric plane of symmetry was not a plane of symmetry for the flow. However, for $W = 0.3$ and 0.7, the flow field is fully symmetrical. It can also be seen that as the heat source length increases, the streamlines break into two circulating cells and the isotherms intensify near the corner of the heat source.

Table 3 presents the values for Nu_m for various heights and lengths of the heat source. For low values of W ($W = 0.05$ and 0.1), the maximum values for Nu_m are obtained for the lowest values of H. Then, Nu_m decreases as H increases. However, for high values of W ($W = 0.3$, 0.5, and 0.7), Nu_m first decreases and then increases as H increases. This is because of the influence of the heat source dimensions on the flow patterns within the enclosure.

6.5. Modified versus original Maxwell models

As mentioned in the introduction, the models used to estimate the properties of the nanofluid significantly affect the heat transfer performance of the nanofluid [15,16]. Yu and Choi [21] argued that the effective thermal conductivity calculated based on the modified Maxwell model is higher than that obtained from the original Maxwell model. The analyses thus far are based on the modified Maxwell model. However, in this section, both the modified and the original Maxwell models are

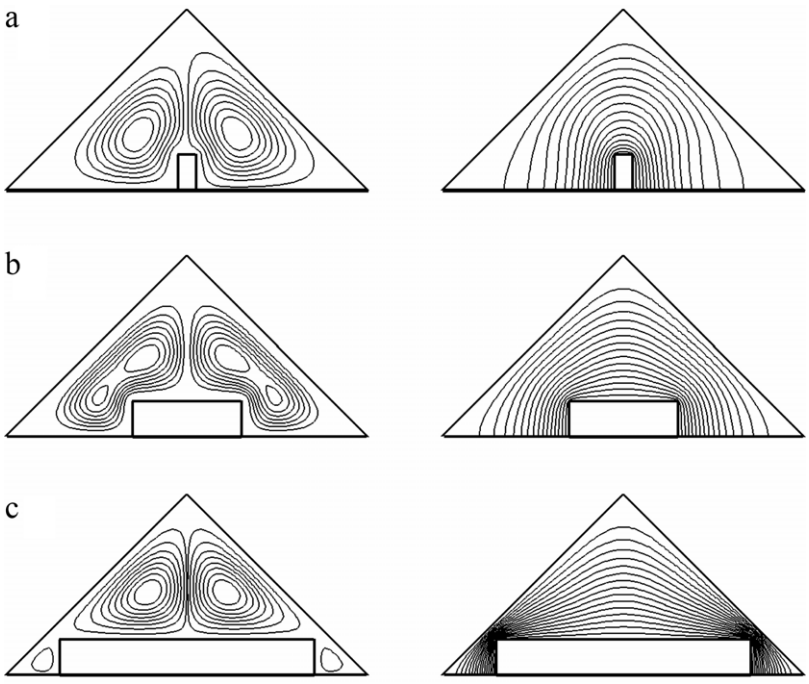

Fig. 12. Streamline (left) and isotherms (right) for Ra $= 10^5$, $\phi = 0.05$, $D = 0.5$, $\delta = 90^\circ$, $H = 0.1$, (a) $W = 0.05$, (b) $W = 0.3$, (c) $W = 0.7$.

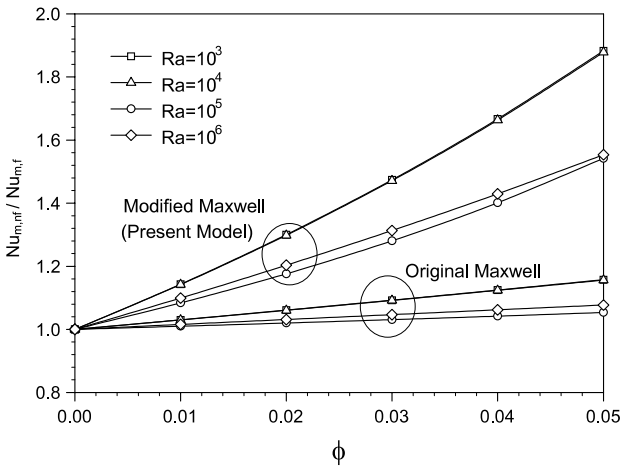

Fig. 13. A comparison between modified and original Maxwell models for the variation of $\mathrm{Nu}_{m,nf}/\mathrm{Nu}_{m,f}$ with ϕ at different Ra.

Table 3
Effects of heat source dimensions (H and W) on average Nusselt number (Nu_m).

	W				
H	0.05	0.1	0.3	0.5	0.7
0.02	18.085	12.420	8.422	7.548	8.249
0.05	12.687	8.785	6.480	6.241	7.425
0.1	10.164	7.235	6.351	6.962	10.183
0.15	8.940	6.526	6.592	8.204	11.950
0.2	8.374	6.293	7.155	6.474	–

used. Fig. 13 presents a comparison between the two models for the variation of the ratio of the nanofluid to the pure fluid average Nusselt numbers ($\mathrm{Nu}_{m,nf}/\mathrm{Nu}_{m,f}$) with respect to ϕ. Both models show an increase in $\mathrm{Nu}_{m,nf}/\mathrm{Nu}_{m,f}$ at higher Ra and ϕ. However, the rate of this increase is more noticeable in the results obtained from the modified Maxwell model.

7. Conclusions

A numerical investigation has been presented to study the natural convection in an isosceles triangular enclosure with a heat source located at its bottom wall and filled with an Ethylene Glycol–Cu nanofluid. The effect of parameters such as Rayleigh number, solid volume fraction, apex angle of the enclosure, position and dimensions of the heat source on the flow and temperature fields as well as the heat transfer rate are examined. A comparison study between the results obtained from the modified and original Maxwell models indicates that the heat transfer rates obtained based on the modified Maxwell model are generally higher than those obtained based on the original Maxwell model.

The enclosure filled with Ethylene Glycol–Cu nanofluid shows a better heat transfer characteristic compared to the enclosure filled with pure Ethylene Glycol. For an isosceles triangular enclosure filled with Ethylene Glycol–Cu nanofluid, an enhanced heat transfer is achieved as the solid volume fraction and Rayleigh number increase. Symmetrical flow and temperature fields are only observed for the right-isosceles triangular enclosure with a relatively long heat source located at the centre of the bottom wall. However, irregularities in the flow and temperature fields are observed when the apex angle is different from 90° or the heat source moves away from the centre of the bottom wall.

At low Rayleigh numbers, the heat transfer rate continuously increases with the enclosure apex angle and decreases with the distance of the heat source from the left vertex. However, at high Rayleigh numbers, the heat transfer rate reaches its minimum at certain values of the apex angle and heat source distance. For shorter heat source length, the highest heat transfer rates are obtained for the lowest heat source height. However, for the longer heat source lengths, the heat transfer rate first decreases and then increases as the heat source height increases.

References

[1] H. Asan, L. Namli, Laminar natural convection in a pitched roof of triangular cross-section: summer day boundary conditions, Energy and Buildings 33 (1) (2000) 69–73.
[2] A. Omri, J. Orfi, S.B. Nasrallah, Natural convection effects in solar stills, Desalination 183 (1–3) (2005) 173–178.
[3] K.A. Joudi, I.A. Hussein, A.A. Farhan, Computational model for a prism shaped storage solar collector with a right triangular cross section, Energy Conversion and Management 45 (3) (2004) 391–409.
[4] E.H. Ridouane, A. Campo, Heightened thermal convection as a result of splitting a square cavity diagonally in half, Journal of Electronic Packaging, Transactions of the ASME 128 (3) (2006) 251–258.
[5] E.H. Ridouane, A. Campo, J.Y. Chang, Natural convection patterns in right-angled triangular cavities with heated vertical sides and cooled hypotenuses, Journal of Heat Transfer 127 (10) (2005) 1181–1186.
[6] R.E. Simons, V.W. Antonnetti, W. Nakayawa, S. Oktay, Heat transfer in electronic packages, in: R. Tummala, et al. (Eds.), Microelectronics Packaging Handbook, 2nd ed., Chapman and Hall, New York, 1997, pp. 315–403.
[7] A. Bar-Cohen, A.A. Watwe, R.S. Prasher, Heat transfer in electronic equipment, in: A. Bejan, A.D. Kraus (Eds.), Heat Transfer Handbook, John Wiley, New York, 2003 (Chapter 13).
[8] A.E. Bergles, Techniques to enhance heat transfer, in: W.M. Rosehnow, et al. (Eds.), Handbook of Heat Transfer, McGraw-Hill, New York, 1999 (Chapter 11).
[9] E.H. Ridouane, A. Campo, Compounded heat transfer enhancement in enclosure natural convection by changing the cold wall shape and the gas composition, Journal of Heat Transfer 129 (7) (2007) 827–834.
[10] S.U.S. Choi, Enhancing thermal conductivity of fluids with nanoparticles, ASME Fluids Engineering Division 231 (1995) 99–105.
[11] E.B. Ogut, Natural convection of water-based nanofluids in an inclined enclosure with a heat source, International Journal of Thermal Sciences 48 (11) (2009) 2063–2073.
[12] E.B. Ogut, Heat transfer of water-based nanofluids with natural convection in a inclined square enclosure, Journal of Thermal Science and Technology 30 (1) (2010) 23–33.
[13] K. Kahveci, Buoyancy driven heat transfer of nanofluids in a tilted enclosure, Journal of Heat Transfer 132 (6) (2010) 1–12.
[14] B. Ghasemi, S.M. Aminossadati, Natural convection heat transfer in an inclined enclosure filled with a water–CuO nanofluid, Numerical Heat Transfer, Part A Applications 55 (8) (2009) 807–823.
[15] C.J. Ho, M.W. Chen, Z.W. Li, Numerical simulation of natural convection of nanofluid in a square enclosure: effects due to uncertainties of viscosity and thermal conductivity, International Journal of Heat and Mass Transfer 51 (17–18) (2008) 4506–4516.
[16] E. Abu-Nada, Effects of variable viscosity and thermal conductivity of Al_2O_3–water nanofluid on heat transfer enhancement in natural convection, International Journal of Heat and Fluid Flow 30 (4) (2009) 679–690.
[17] J. Koo, C. Kleinstreuer, A new thermal conductivity model for nanofluids, Journal of Nanoparticle Research 6 (6) (2004) 577–588.
[18] R. Prasher, P. Bhattacharya, P.E. Phelan, Thermal conductivity of nanoscale colloidal solutions (nanofluids), Physical Review Letters 94 (2) (2005) 1–4.
[19] S.M.S. Murshed, K.C. Leong, C. Yang, A combined model for the effective thermal conductivity of nanofluids, Applied Thermal Engineering 29 (11–12) (2009) 2477–2483.
[20] J.C. Maxwell, A Treatise on Electricity and Magnetism, vol. II, Oxford University Press, Cambridge, UK, 1873, p. 54.
[21] W. Yu, S.U.S. Choi, The role of interfacial layers in the enhanced thermal conductivity of nanofluids: a renovated Maxwell model, Journal of Nanoparticle Research 5 (1–2) (2003) 167–171.
[22] E. Fuad Kent, Numerical analysis of laminar natural convection in isosceles triangular enclosures for cold base and hot inclined walls, Mechanics Research Communications 36 (4) (2009) 497–508.
[23] T. Basak, S. Roy, S.K. Babu, A.R. Balakrishnan, Finite element analysis of natural convection flow in a isosceles triangular enclosure due to uniform and non-uniform heating at the side walls, International Journal of Heat and Mass Transfer 51 (2008) 4496–4505.
[24] A. Omri, M. Najjari, S.B. Nasrallah, Numerical analysis of natural buoyancy-induced regimes in isosceles triangular cavities, Numerical Heat Transfer, Part A Applications 52 (7) (2007) 661–678.
[25] G.A. Holtzman, R.W. Hill, K.S. Ball, Laminar natural convection in isosceles triangular enclosures heated from below and symmetrically cooled from above, Journal of Heat Transfer 122 (3) (2000) 485–491.
[26] Y. Varol, H.F. Oztop, A. Koca, Entropy production due to free convection in partially heated isosceles triangular enclosures, Applied Thermal Engineering 28 (2008) 1502–1513.
[27] E.F. Kent, Numerical analysis of laminar natural convection in isosceles triangular enclosures, Proceedings of the Institution of Mechanical Engineers, Part C: Journal of Mechanical Engineering Science 223 (5) (2009) 1157–1169.
[28] C. Lei, S.W. Armfield, J.C. Patterson, Unsteady natural convection in a water-filled isosceles triangular enclosure heated from below, International Journal of Heat and Mass Transfer 51 (11–12) (2008) 2637–2650.

[29] E.H. Ridouane, A. Campo, Formation of a pitchfork bifurcation in thermal convection flow inside an isosceles triangular cavity, Physics of Fluids 18 (7) (2006) Article Number: 074102 2006.
[30] E.F. Kent, E. Asmaz, S. Ozerbay, Laminar natural convection in right triangular enclosures, Heat and Mass Transfer/Waerme-und Stoffuebertragung 44 (2) (2007) 187–200.
[31] C.S. Kim, K. Okuyama, J. Fernandez De La Mora, Performance evaluation of an improved particle size magnifier (PSM) for single nanoparticle detection, Aerosol Science and Technology 37 (10) (2003) 791–803.
[32] E. Abu-Nada, Z. Masoud, A. Hijazi, Natural convection heat transfer enhancement in horizontal concentric annuli using nanofluids, International Communications in Heat and Mass Transfer 35 (5) (2008) 657–665.
[33] H.C. Brinkman, The viscosity of concentrated suspensions and solutions, Journal of Chemical Physics 20 (1952) 571–581.
[34] S. Palm, G. Roy, C.T. Nguyen, Heat transfer enhancement with the use of nanofluids in a radial flow cooling system considering temperature dependent properties, Applied Thermal Engineering 26 (2006) 2209–2218.
[35] H.F. Oztop, E. Abu-Nada, Numerical study of natural convection in partially heated rectangular enclosures filled with nanofluids, International Journal of Heat and Fluid Flow 29 (5) (2008) 1326–1336.
[36] A. Akbarinia, A. Behzadmehr, Numerical study of laminar mixed convection of a nanofluid in horizontal curved tubes, Applied Thermal Engineering 27 (2007) 1327–1337.
[37] S.V. Patankar, Numerical Heat Transfer and Fluid Flow, Hemisphere Publishing Corporation, Taylor and Francis Group, New York, 1980, pp. 113–137.
[38] Y. Varol, A. Koca, H.F. Oztop, Natural convection in a triangle enclosure with flush mounted heater on the wall, International Communications in Heat and Mass Transfer 33 (8) (2006) 951–958.
[39] S.M. Aminossadati, B. Ghasemi, Natural convection cooling of a localised heat source at the bottom of a nanofluid-filled enclosure, European Journal of Mechanics—B/Fluids 28 (2009) 630–640.
[40] B. Ghasemi, S.M. Aminossadati, Periodic natural convection in a nanofluid-filled enclosure with oscillating heat flux, International Journal of Thermal Sciences 49 (1) (2010) 1–9.
[41] B. Ghasemi, S.M. Aminossadati, Brownian motion of nanoparticles in a triangular enclosure with natural convection, International Journal of Thermal Sciences 49 (6) (2010) 931–940.